Crossover from "gas-like" to "liquid-like" molecular diffusion in a simple supercritical fluid

Umbertoluca Ranieri, Mario Santoro, Ferdinando Formisano, Michael Marek Koza, Federico A Gorelli, Alessio de Francesco, Livia E Bove

Crossover from "gas-like" to "liquid-like" molecular diffusion in a simple supercritical fluid

Umbertoluca Ranieri[1,2], Ferdinando Formisano[3,4*], Federico A. Gorelli[5,6,7*], Mario Santoro[5,6], Michael Marek Koza[4], Alessio De Francesco[3,4] and Livia E. Bove[1,8,9]

[1]Dipartimento di Fisica, Università di Roma La Sapienza, Roma, Italy.
[2]Centre for Science at Extreme Conditions and School of Physics and Astronomy, University of Edinburgh, EH9 3FD Edinburgh, UK.
[3]CNR-IOM & INSIDE@ILL c/o Operative Group in Grenoble (OGG), Grenoble Cedex 9, France.
[4]Institut Laue-Langevin, Grenoble Cedex 9, France.
[5]Consiglio Nazionale delle Ricerche, Istituto Nazionale di Ottica, CNR-INO, Via Nello Carrara 1, Sesto Fiorentino (FI), 50019, Italy.
[6]European Laboratory for Nonlinear Spectroscopy, LENS, Via Nello Carrara 1, Sesto Fiorentino (FI), 50019, Italy.
[7]Center for High Pressure Science and Technology Advanced Research (HPSTAR), 1690 Cailun Road, Shanghai, 201203, China.
[8]Laboratory of Quantum Magnetism, Institute of Physics, École Polytechnique Fédérale de Lausanne, Lausanne, CH-1015, Switzerland.
[9]Institut de Minéralogie, de Physique des Matériaux et de Cosmochimie, Sorbonne Université, UMR CNRS 7590, Paris, France.

*Corresponding author(s). E-mail(s): formisan@ill.fr; gorelli@lens.unifi.it;
Contributing authors: umbertoluca.ranieri@uniroma1.it; santoro@lens.unifi.it; koza@ill.fr; defrance@ill.fr; liviaeleonora.bove@uniroma1.it;

Abstract

According to textbooks, no physical observable can be discerned allowing to distinguish a liquid from a gas beyond the critical point. Here we report

quasi-elastic neutron scattering measurements of the molecular self diffusion in supercritical fluid methane as a function of pressure along the 200 K isotherm (corresponding to 1.05 times the critical temperature) where we observe a clear crossover in the dynamic structure factor from a gas-like Gaussian to a liquid-like Lorentzian signal. The crossover is progressive and takes place upon compression at about the Widom line intercept. Concurrently, a sharp change in the pressure dependence of the molecular self-diffusion coefficient takes place. At considerably higher pressures, we find that the same liquid-like jump diffusion mechanism can fit the experimental data on both sides of the Frenkel line, marking the change from a non-rigid to a rigid fluid. The observation of a gas-like to liquid-like dynamical crossover in supercritical methane could have planet-wide implications, and possible industrial applications in green chemistry.

Keywords: supercritical fluids, neutron scattering, molecular diffusion, high pressure

Matter can be pushed to temperatures and pressures above those of its critical point, in a state, called supercritical fluid (SCF), where we are unable to distinguish whether the system is a liquid or a gas. As a result, supercritical fluids possess an intimate hybrid nature: they are said to have the capability to effuse "like a gas" but to dissolve materials "like a liquid". This makes them used in the most disparate industrial processes, such as pharmaceutical and cosmetics processing, extracting essential oils, dissolving waste material, brewing or decaffeinating coffee beans without leaving toxic residues. In particular, near the critical point, small changes in pressure or temperature result in large changes in density, allowing many properties of a supercritical fluid to be "fine-tuned" in such processes [1–6].

Understanding the physical behaviour of supercritical fluids is not only important for industrial applications but also to gain a much better knowledge of what goes on deep inside giant planets like Jupiter, Saturn, Uranus or Neptune. As we delve into their atmosphere, we may indeed encounter simple matter in the supercritical fluid state [7, 8]. This will determine not only their thermal properties, and in particular the way heat is stored and flows around planets, but also the anomalous solubility of other volatiles in their atmosphere [9, 10], as well as other surprising phenomena such as the separation of Uranus atmosphere from its interior, recently suggested by the anomalously low heat flow measurements from the Voyager spacecraft [11]. Considering the number of exoplanets and super-Earths that are being discovered, many of them larger and with more extreme environments than found in our own solar system, the possibility for supercritical fluids to be found in planetary environments is only set to increase. Furthermore, SCFs with gas-like viscosity as well as melt-like wetting and element-carrying capability are an ideal agent for chemical transport at subduction zones and could play a role as life-sustaining solvents on other worlds [12, 13].

Above the critical temperature, no increase in pressure can liquefy the system and when the pressure is greatly increased, a supercritical fluid of much higher density, close to the one of a solid, is produced. The significant changes in density observed close to the critical point are expected to correlate with changes in other properties of the fluid. The question scientists have long debated is: may a region of the pressure-temperature (P-T) plane and a physical observable be discerned allowing to unambiguously distinguish between a gas-like and liquid-like behaviour in the supercritical fluid?

Two different scenarios have been recently put forward as an answer to this question. The first one indicates the Widom line, i.e. the line emanating from the critical point which represents the maxima/minima in certain thermophysical properties, as the line separating a gas-like behaviour from a liquid-like behaviour in the SCF. A crossover in the anomalous dispersion (i.e. the difference between the unrelaxed and relaxed value) of the simulated THz sound velocity [14–16], the observation of a pseudo-boiling phenomenon [17] and of droplet formation [18], and a change in density fluctuations correlations [19–21] have been reported to occur when crossing the Widom line. The second scenario rather envisages the Frenkel line, i.e. the line along which the structural relaxation time equals the shortest period of transverse oscillations of the particles (atoms or molecules) within the system [22–26], as the line separating a solid-like (rigid) diffusive behaviour of the fluid from a gas-like (non-rigid) one. At high pressures above the Frenkel line, with the exception that the particles occasionally hop from one position to another, dense SCFs somehow behave like solids. They can sustain transverse acoustic excitations and show a velocity autocorrelation function which monotonically decays to zero.

Here we report a quasi-elastic neutron scattering (QENS) study of supercritical methane as a function of pressure at a constant temperature of 200 K (just above the critical temperature of 190.55 K), providing a direct measurement of the molecular diffusion in the system. We find that the measured self-dynamic structure factor, i.e. the space and time Fourier transform of the self pair correlation function [27], shows a clear change from a Gaussian lineshape, describing the molecular diffusion in a gas, to a Lorentzian lineshape, describing the molecular diffusion in a liquid. The change is completed when pressure crosses the Widom line along the 200 K isotherm and no further changes are observed at higher pressures, for example when crossing the Frenkel line. The molecular diffusion coefficient has been determined over a range of densities covering almost three orders of magnitude and compared to both (non-ideal) gas and dense-fluid theoretical descriptions. Its variation as a function of pressure shows a clearcut slowing down when crossing the Widom line, reminiscent of the change in the fluid compressibility. The observation of this crossover in supercritical methane could have planet-wide implications, in particular due to the ubiquitous presence of methane in our solar system. The existence of a non-homogeneous supercritical state in gas, like methane, constituting gas-giants, will indeed determine if a boundary between the planet's interior and its atmosphere can be defined. This would impact

planetary properties such as the thermal conductivity and other heat-related physical phenomena like storm activity, as well as mass diffusion related properties like the ionic conductivities and consequent generation of anomalous magnetic fields [28–30].

Experiments

Figure 1 reports the temperature-pressure phase diagram of methane. The critical point is at T_C=190.55 K and P_C= 46 bar. Data at seventeen pressures between 8.5 and 2450 bar were acquired for this study along the 200 K isotherm (1.05 T_C), six below and eleven above P_C. The used high-pressure setup is described in the Methods section. The pressure range corresponds to a huge density variation, from 0.00868 g cm^{-3} at 8.5 bar to 0.47101 g cm^{-3} at 2450 bar (5000% of the initial value). The first value is only an order of magnitude higher than the density of gas methane at ambient pressure (0.00097 g cm^{-3} at 200 K). The second value is comparable to the density of liquid methane (for example, 0.4389 g cm^{-3} at ambient pressure and 100 K). Density values used throughout this paper are taken from the equation of state of the online National Institute of Standards and Technology (NIST) Reference Fluid Thermodynamic and Transport Properties Database, which uses ref. [31].

The pressure dependence of the density along the 200 K isotherm is also reported in Fig. 1 (upper panel). The intercepts of the Widom line and of the Frenkel line with the 200 K isotherm are at 59 and 670 bar, respectively [24, 31]. The criterion chosen to locate the Frenkel line in ref. [24] is the disappearance of the first minimum of the calculated velocity autocorrelation function. Figure 1 anticipates the main result of this study: We observe a crossover in the lineshape of the experimental spectra (proportional to the self-dynamic structure factor of the system) from Gaussian to Lorentzian upon pressure increase, which is completed above the Widom line intercept.

Figure 2 depicts examples of QENS spectra of the sample, plotted as a function of the energy transfer E, for a few selected P and Q values, Q being the modulus of the wavevector transfer. It is well-known that because of the very large incoherent neutron scattering cross section of ^{1}H, the QENS signal from CH_4 is dominated by the *self* (single-particle) dynamics of the molecules. In particular, the *translational* self-dynamic structure factor was measured in the present study. The (quasi-elastic) signal monotonically gets broader either with decreasing pressure at constant Q (see Supplementary Fig. 1) or with increasing Q at constant P (see below), as expected in case of translational motion. As can be seen in Fig. 2, spectra are best fitted by a Gaussian function at low pressures and by a Lorentzian function at high pressures. The Gaussian-to-Lorentzian transition is progressive. Gaussian fits were preferred for the data at pressures up to 51.5 bar and Lorentzian fits were preferred at and above 67.5 bar. More details about the extraction of spectra from the raw data and about the fitting of the spectra are given in the Methods section.

Data analysis

In dilute fluids, the frequency of the collisions between particles is low and the particles experience a ballistic motion between two collisions. As a consequence, a velocity and a trajectory can be defined and the mean square displacement (MSD) of the particle displays a t^2 time dependence. This behaviour translates, when switching to the experimental domain (Q, ω), into the free-particles (ideal gas) expression for the self-dynamic structure factor $S_{\rm self}(Q, \omega)$ given by [27]:

$$S_{\rm self}(Q,\omega) = \left(\frac{m}{2\pi k_B T Q^2}\right)^{1/2} \exp\left(-\frac{m\omega^2}{2k_B T Q^2}\right), \tag{1}$$

which is a Gaussian function of the frequency ω (ω=$E/\hbar$) centered at ω=0, whose width increases linearly with Q. Here, m is the mass of the particle and $k_{\rm B}$ the Boltzmann constant. $2k_{\rm B}T/m$ gives the mean square velocity of the diffusing particles. The self-diffusion coefficient D is given by the kinetic Chapman-Enskog theory for a dilute fluid composed of hard spheres and can be approximated for the non-dilute hard-sphere fluid by [32–34]:

$$D = \frac{1.01896}{g(\sigma)} \frac{3}{8n\sigma^2} \left(\frac{k_{\rm B}T}{\pi m}\right)^{1/2}, \tag{2}$$

with the numerical factor 1.01896 being a result of using the ninth Enskog approximation, $g(r)$ being the radial distribution function, σ the spheres diameter, and n the number density. Eq. 2 is almost exact in the low-density limit while its applicability at higher densities has been thoroughly tested in molecular dynamics calculations [33]. For the range over which Gaussian fits were employed in the present study, i.e. for a packing fraction ζ=$\pi n\sigma^3/6$ up to about 0.1, Eq. 2 is accurate within 10% compared to recent computational values for hard spheres [35, 36]. On the other hand, there is extensive literature [37, 38] showing that the hard-sphere model correctly reproduces the experimental diffusion coefficient of methane at such modest pressures, provided that the equivalent hard-sphere diameter is a free fitting parameter. It follows that the free-particles expression of Eq. 1 can be extended at higher densities using Eq. 2 and the Gaussian $S_{\rm self}(Q, \omega)$ writes now as:

$$S_{\rm self}(Q,\omega) = \left(\frac{\ln(2)}{\pi\Gamma_G^2(Q)}\right)^{1/2} \exp\left(-\frac{\ln(2)\omega^2}{\Gamma_G^2(Q)}\right), \tag{3}$$

$$\text{where} \qquad \Gamma_G(Q) = KQ. \tag{4}$$

The values of the half width at half maximum $\Gamma_G(Q)$ obtained from the Gaussian fits of our spectra display a clear linear trend with Q, as shown in Fig. 3a, where the data are reported together with their linear fit. From the values of the fitted slope K, reported in Extended Data Figure 1 at each investigated pressure, we obtained D in the gas-like regime using K=$\frac{8}{3}\frac{(2\pi\ln(2))^{1/2}}{1.01896} n\sigma^2 g(\sigma) D$ as obtained by comparing Eqs. 1 to 4, $g(\sigma)$=$\frac{1-\frac{\zeta}{2}}{(1-\zeta)^3}$ as given by the widely

employed Carnahan–Starling equation of state [39], and σ=3.61 Å as given for methane at 200 K by NMR measurements of D [38]. The self-diffusion coefficient is plotted in Fig. 4 as a function of pressure.

When the density further increases and becomes comparable to the one of a liquid, the collision frequency also strongly increases and the particles experience several multiple uncorrelated collisions during the typical experimental timescales, giving rise to a random Brownian motion characterized by a linear, and not anymore quadratic, time dependence for the MSD [40, 41]. As a consequence the self-dynamic structure factor has a Lorentzian shape centered at ω=0, i.e.:

$$S_{\mathrm{self}}(Q,\omega) = \frac{1}{\pi}\frac{\Gamma_L(Q)}{\omega^2+\Gamma_L^2(Q)}, \tag{5}$$

which is the model customarily used to analyze QENS data on bulk liquid samples. Typically, the half width at half maximum $\Gamma_L(Q)$ is observed to be proportional to Q^2 at small Q (as expected for Fickian diffusion) and to lie below that expectation at high Q, i.e., when one is probing shorter distances and the microscopic details of the motion become relevant. It is often correctly described by the formula:

$$\Gamma_L(Q) = \frac{DQ^2}{1+\tau DQ^2}. \tag{6}$$

Eqs. 5 and 6 were previously employed in many QENS studies, including studies of liquid methane [42], supercritical methane at liquid densities [43], and high-pressure interfacial methane [44], as well as studies of other dense fluids such as for example liquid water over wide ranges of temperature and pressure [45, 46]. Eq. 6 is known to be associated to the jump-like nature of the translational motion in dense systems, typically because of the presence of a cage effect, and τ represents the time spent by the diffusing particle at quasi-equilibrium sites between rapid jumps [47]. Figure 3b reports the half width of the Lorentzian fits of our spectra as a function of Q at each investigated pressure as well as its best fits using Eq. 6, from which we extracted values of τ and D in the liquid-like regime, reported in Fig. 4.

Results

As can be seen in Fig. 4, τ shows a 20% decrease with increasing pressure attaining a minimum at around the Frenkel line intercept (670 bar) followed by a small 10% increase above that pressure. However, the estimation of the residence time τ is dominated by the high-Q values of $\Gamma_L(Q)$; its uncertainty can be significant for different reasons, such as a high background. Figure 4 also plots the obtained self-diffusion coefficient D as a function of pressure and values range from $1481.1\times10^{-9}\mathrm{m^2s^{-1}}$ at 8.5 bar to $6.8\times10^{-9}\mathrm{m^2s^{-1}}$ at 2450 bar. At our highest pressure, the value of D is close to the typical values of liquid methane (for example, $3.6\times10^{-9}\mathrm{m^2s^{-1}}$ at 1.5 bar and 102 K [42]). In Fig. 4, the diffusion coefficient is compared with NMR data of methane at the same

temperature of 200 K [48] and with a literature computational (molecular dynamics) prediction for hard spheres [36]. The hard-sphere prediction [36] reproduces the trend of the measured diffusion coefficient fairly well over the entire pressure range, and this for a P-independent value of the sphere diameter σ of 3.61 Å. This is at variance with our earlier QENS work on methane [43], where we reached the (much higher) freezing pressure of 1.4 GPa at 300 K and observed failure of the hard-sphere model.

The largest relative deviations between our data and the hard-sphere prediction are for the intermediate pressure range (40-80 bar), and this is likely to be associated to the existence of a pressure regime where both the Gaussian and Lorentzian modelling of the dynamic structure factor are not fully justified yet representing the only models, though approximate, presently available to describe the diffusive dynamics. Consistently, this is also the pressure range where the fits of the wavevector transfer dependence of the Gaussian and Lorentzian half widths are less satisfactory. It can be also noticed that the Gaussian and Lorentzian fits to our spectra are of comparable quality at about 40-50 bar and none of them perfectly reproduces the lineshape of the experimental spectra (see Fig. 2). However, while the Gaussian fits provide reasonable values for D, the Lorentzian fits provide unreasonably small values compared to the literature experimental values [48] and to the hard-sphere predictions [36] at all pressures below 67.5 bar. For example, at 51.5 bar, Lorentzian fits provide D=50.7×10^{-9}m^{2}s^{-1}, to be compared with 89.4×10^{-9}m^{2}s^{-1} for the Gaussian fits. This clearly indicates that the Gaussian description is more appropriate than the Lorentzian one up to 51.5 bar. Above 51.5 bar, the situation is reversed, with i) the Gaussian fits providing unreasonably small diffusion coefficient values (for example at 67.5 bar, 36.0 ×10^{-9}m^{2}s^{-1} for the Lorentzian and 23.5 ×10^{-9}m^{2}s^{-1} for the Gaussian fits) and ii) the Lorentzian fits clearly describing the measured spectra much better (see Fig. 2). To further support our choice of employing Gaussian fits up to 51.5 bar and Lorentzian fits at and above 67.5 bar, the likeliness of the obtained diffusion coefficient is better quantified in the Supplementary Information (Supplementary Note 1 and Figs. 2,3), where we also report the results of a Bayesian analysis [49] of the experimental spectra (Supplementary Note 2 and Figs. 4–9).

Finally, we calculated the product of the self-diffusion coefficient D with the shear viscosity η (see Extended Data Figure 2), using the literature estimation of η given by the NIST Reference Fluid Thermodynamic and Transport Properties Database, which uses ref. [50]. The Stokes–Einstein–Sutherland (SES) relation, which is commonly used in the literature of atomic and molecular liquids, predicts a constant product $D\eta$ along isotherms. In our case, the product clearly shows two regimes along the 200 K isotherm: while below the pressure of intercept with the Widom line, $D\eta$ decreases with increasing pressure and the SES relation is violated, above that pressure, $D\eta$ is constant with pressure and the SES relation holds. Experimental literature data showed that $D\eta$ is constant within the experimental uncertainties in compressed liquid methane along the low-temperature isotherms 110, 140 and 160 K [38], as reported for

example in our previous work [43] (Supplementary Figure 5), but significantly increases with pressure in very dense supercritical methane along the room-temperature isotherm [43]. On the other hand, the SES relation is typically not expected to hold at low pressures below twice the critical density. It is a well-known result of isomorph theory [51], experiments of various simple fluids, and simulations of hard spheres and of the Lennard-Jones system [35, 36] that the product $D\eta$ cannot be constant over isotherms in the gas phase.

Final comments

The fundamental problem of distinguishing between a gas-like and a liquid-like region in the phase diagram of simple supercritical fluids has fed a high-pitched debate in the literature [14–26]. In the present measurements, we establish the existence of a crossover in the self-dynamic structure factor of SCF methane measured by QENS along the 200 K isotherm. The change from a Gaussian to a Lorentzian lineshape indicates the crossover from a gas-like to a liquid-like diffusive dynamics of the molecules and occurs roughly at the pressure at which the Widom line intercepts the 200 K isotherm, indicating that the Widom line separates gas-like and liquid-like behaviours as concerns the self diffusion of CH_4 in the vicinity of the critical temperature. This result is exclusively based upon the experimental determination of a basic transport property as a function of the pressure and use the only available diffusive models available in literature, without resorting to any other external input or calculations.

To our knowledge, the present work represents the first to employ the QENS technique to investigate a SCF sample in the vicinity of its critical point. The advantage of using neutrons to investigate the diffusion in a SCF resides in the fact that neutron scattering is a weak process and the sample response is linear. It follows that the measured dynamic structure factor is determined by the spectrum of the spontaneous correlations between molecules, and thus gives a fundamental information on the molecular interaction [52]. Along the thermodynamic path we followed, we could cross both the Widom and the Frenkel line. The picture that emerges is that at pressures below the Widom line, the molecular diffusion is basically governed by the harsh repulsive forces between molecules while the weaker, longer-ranged attractive forces have little influence on the dynamics. The system can be described as a dense (non-ideal) gas. Conversely, above the Widom line, the sharp increase in density makes the free path of the molecules to strongly decrease and the diffusion mechanism becomes sensitive to the longer-ranged molecular interaction and depends on the average molecular distances. The molecular diffusion can be thus described as that of a liquid and the Stokes–Einstein–Sutherland relation holds. This happens starting from much lower densities (by approximately a factor of 2) than those typical for liquid methane.

The presence of a Frenkel line does not seem to affect in a radical way the pressure dependence of the diffusion coefficient nor the diffusion mechanism probed in the present measurements, with the exception of a shallow minimum

in the trend of the in-cage molecular residence time τ as a function of pressure. On the "non-rigid fluid" side of the Frenkel line, a competition between the repulsive potential and attractive Van der Waals forces between adjacent molecules undergoing diffusion is in place. Attractive Van der Waals forces dominate in the fluid at the lowest densities and lead the in-cage residence time of the molecules to decrease upon pressure increase [53]. Conversely, when crossing the Frenkel line, τ increases with pressure because of the major role of the repulsive potential and the consequent stabilisation of the neighbour's cage. As a consequence, the variation of the residence time as a function of pressure in an isothermal experiment can display a minimum as one proceeds from the non-rigid to the rigid fluid. Future studies will be able to verify whether this intriguing observation is reproduced and matches the Frenkel line intercepts also along other isotherms. At pressures above the Frenkel line, the (relatively) close packed arrangement of the molecules determines a much stronger interaction between close neighbour molecules and the onset of long-living density fluctuation modes as well as of shear modes. The diffusion mechanism progressively becomes more similar to the hopping observed in solids through vacancies and the system can be described as a "rigid" liquid on the short timescales here explored.

Concerning the Widom line, it is worth recalling that there is a group of lines emanating from the critical point which are associated with maxima/minima in different thermophysical properties such as the speed of sound, isothermal compressibility, isochoric and isobaric heat capacities, which have all been named "Widom lines" [54]. Close to the critical point, as in the present experiment, the choice of the specific thermophysical property is relatively unimportant as all of the maxima/minima closely coincide, but far away from the critical point, the maxima in the response functions begin to deviate significantly from each other. However, it is now generally agreed that the Widom line can be identified to a maximum in the correlation length characterizing the range of the molecular interactions which is here directly probed through the dynamic structure factor. In this extent, the dynamic structure factor turns out to be a pertinent physical observable allowing us to distinguish between a gas-like and a liquid-like behaviour within the supercritical fluid. Its change in lineshape when crossing the Widom line reflects a substantial change in the molecular interaction length scale with clear consequences in the transport properties of the system. This observation could have major consequences on the geodynamics of gas giant planets in our Solar System and beyond, and could be exploited to tailor the efficiency of supercritical fluids in industrial applications. It remains to be established how a planet-scale crossover through the Widom line would affect heat flow, like it is observed for Uranus.

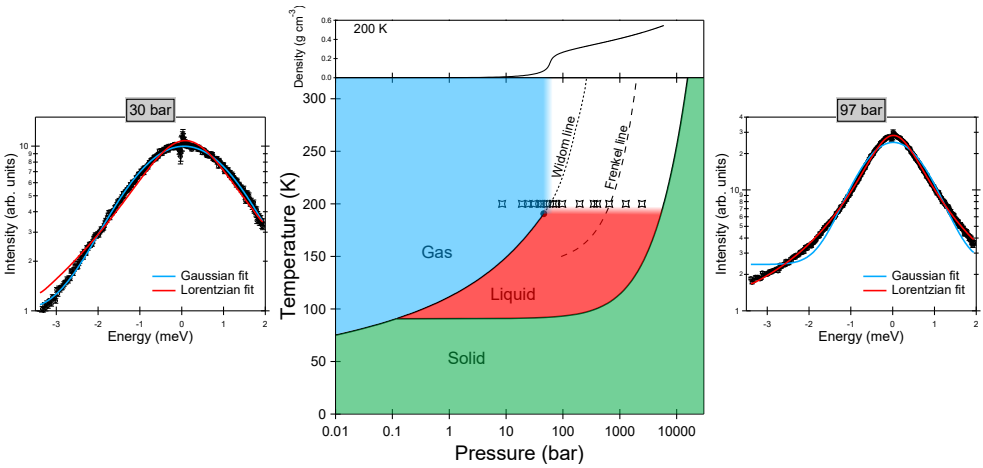

Fig. 1: **Phase diagram of methane.** Temperature-pressure phase diagram of methane including the Widom line (locus of the isobaric heat capacity maxima [31]) and the predicted Frenkel line from ref. [24]. The critical point is at 190.55 K and 46 bar. Symbols depict the pressure points measured (along the 200 K isotherm) in the present experiment. The density profile at 200 K from ref. [31] is reported on top of the phase diagram. Examples of QENS experimental spectra in logarithmic scale (empty circles) at two selected pressures on each side of the Widom line are also reported with their best Gaussian/Lorentzian fits (solid lines) to highlight the Gaussian-to-Lorentzian crossover upon compression. To improve statistics, these two spectra were obtained by summing up measurements in the 0.55–0.85 Å^{-1} exchanged wavevector range.

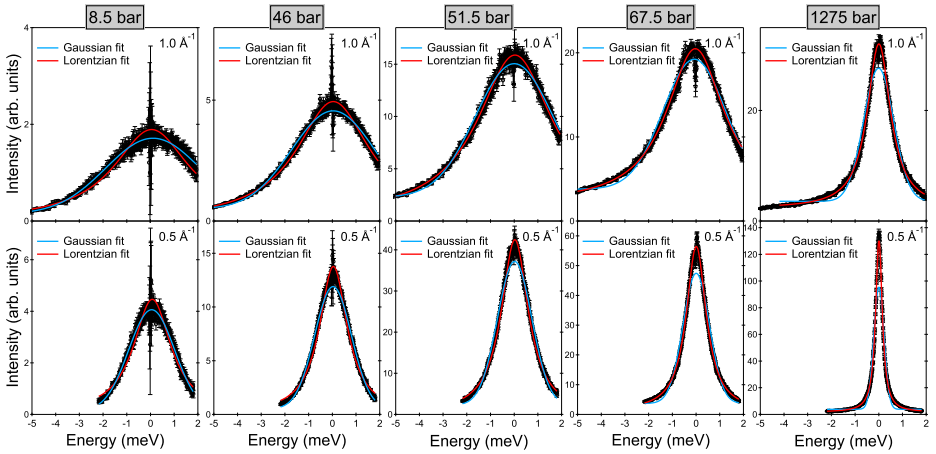

Fig. 2: **Examples of QENS spectra.** QENS spectra of the sample at 200 K at the indicated pressure and wavevector transfer values, collected using an incoming neutron wavelength of 5.12 Å and an instrumental resolution of full width at half maximum equal to 0.077 meV. Experimental data (empty circles) are compared to the best Gaussian and Lorentzian fits (solid lines).

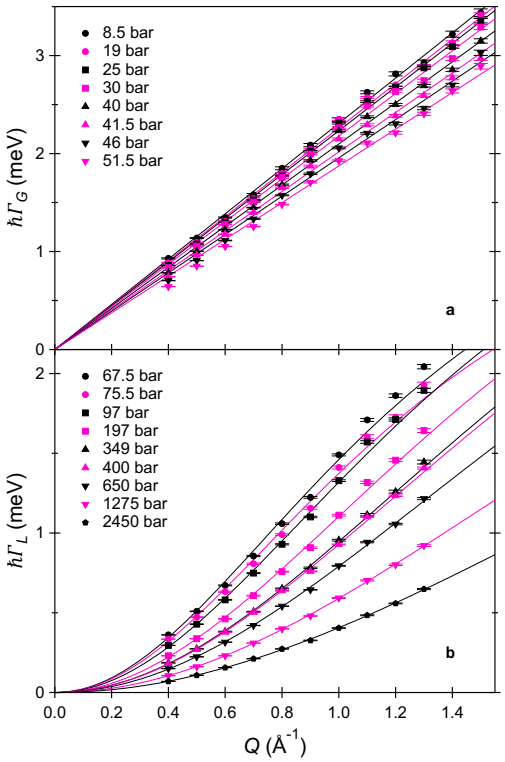

Fig. 3: **Wavevector transfer dependence of Γ_G and Γ_L.** Fitted Gaussian (panel **a**) or Lorentzian (panel **b**) half widths at half maximum (symbols) as a function of Q, at all investigated pressures. The best fits to the data at each pressure are shown as solid lines. For the Gaussian half widths, the fits are lines passing through zero whose slopes allowed us to extract D (see Eq. 4 and following discussion). The Lorentzian half widths were modelled using Eq. 6 with τ and D as free parameters.

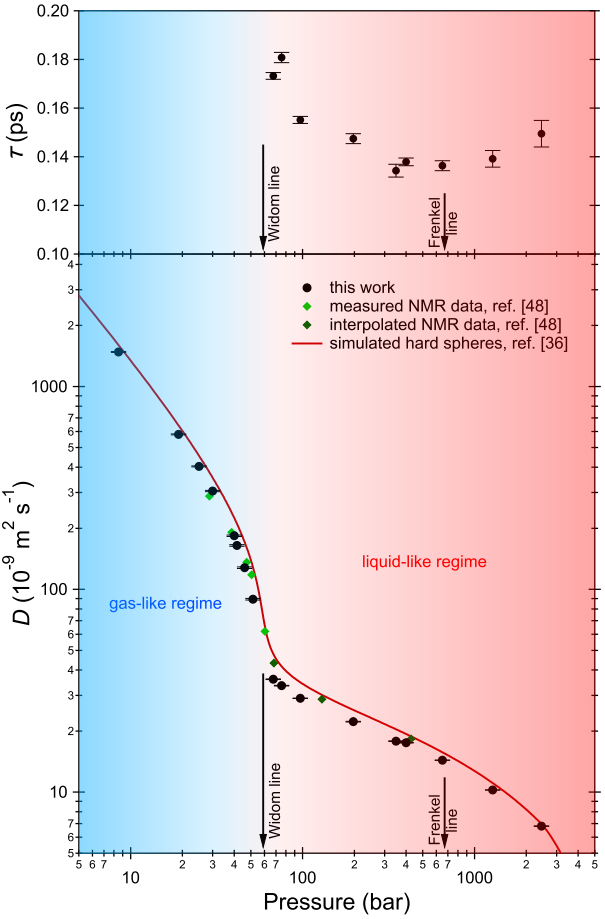

Fig. 4: **Pressure dependence of the mean residence time and of the diffusion coefficient at 200 K.** Top panel: Parameter τ of the jump diffusion model as obtained from the fits shown in Fig. 3b. Bottom panel: Self-diffusion coefficient D (full circles) as obtained from the fits shown in Fig. 3. A gas-like (resp. liquid-like) regime is defined as being the regime where D was obtained using Gaussian (resp. Lorentzian) fits and the two regimes are indicated with different colors, with the blur in between indicating that the Gaussian-to-Lorentzian transition is progressive. The arrows indicate the intercepts of the Widom and Frenkel lines with the 200 K isotherm. We also report i) experimental NMR values for methane at 200 K (full diamonds) measured in ref. [48] or obtained in ref. [48] from interpolation of data measured at other temperatures and ii) simulated values for the hard sphere fluid from ref. [36] (full line), plotted here using T=200 K, σ=3.61 Å, and the mass of the methane molecule.

References

[1] Johnston, K.P., Shah, P.S.: Making nanoscale materials with supercritical fluids. Science **303**, 482–483 (2004)

[2] De Simone, J.M.: Practical approaches to green solvents. Science **296**, 799–803 (2002)

[3] Agregán, R., Bangar, S.P., Hassoun, A., Hano, C., Pateiro, M., Lorenzo, J.M.: Green Technologies for Sustainable Food Production and Preservation: Supercritical Fluids. Reference Module in Food Science, 1–15 (2023)

[4] Qian, L., Wang, S., Xu, D., Guo, Y., Tang, X., Wang, L.: Treatment of municipal sewage sludge in supercritical water: a review. Water Research **89**, 118–131 (2016)

[5] Correa, C.R., Kruse, A.: Supercritical water gasification of biomass for hydrogen production review. J. Supercrit. Fluids **133**, 573–590 (2018)

[6] Chan, H.K., Kwok, P.C.L.: Production methods for nanodrug particles using the bottom-up approach. Adv. Drug Deliv. Rev. **63**, 406–416 (2011)

[7] Fortney, J.J., Nettelmann, N.: The Interior Structure, Composition, and Evolution of Giant Planets. Space Sci Rev **152**, 423–447 (2010)

[8] Alibert, Y., Mousis, O., Mordasini, C., Benz, W.: New Jupiter and Saturn Formation Models Meet Observations. Astrophys. J. **626**, 57 (2005)

[9] Duan, Z., Sun, R.: An improved model calculating CO2 solubility in pure water and aqueous NaCl solutions from 273 to 533 K and from 0 to 2000 bar. Chemical Geology **193**, 257 (2003)

[10] Ni, H., Zhang, L., Xiong, X., Mao, Z., Wang, J.: Supercritical fluids at subduction zones: Evidence, formation condition, and physicochemical properties. Earth-Science Reviews **167**, 62–71 (2017)

[11] Mousis, O., *et al.*: Scientific rationale for Uranus and Neptune in situ explorations. Planetary and Space Science **155**, 12–40 (2018)

[12] Eckert, C.A.: Supercritical fluids as solvents for chemical and materials processing. Nature **383**, 313–318 (1996)

[13] Scott, S., Driesner, T., Weis, P.: Geologic controls on supercritical geothermal resources above magmatic intrusions. Nat. Commun. **6**, 7837 (2015)

[14] Simeoni, G.G., Bryk, T., Gorelli, F., Krisch, M., Ruocco, G., Santoro, M.,

Scopigno, T.: The Widom line as the crossover between liquid-like and gas-like behaviour in supercritical fluids. Nature Phys. **6**, 503–507 (2010)

[15] Bryk, T., Gorelli, F., Ruocco, G., Santoro, M., Scopigno, T.: Collective excitations in soft-sphere fluids. Phys. Rev. E **90**, 042301 (2014)

[16] Gorelli, F.A., Bryk, T., Krisch, M., Ruocco, G., Santoro, M., Scopigno, T.: Dynamics and thermodynamics beyond the critical point. Sci. Rep. **3**, 1203 (2013)

[17] Maxim, F., Contescu, C., Boillat, P., Niceno, B., Karalis, K., Testino, A., Ludwig, C.: Visualization of supercritical water pseudo-boiling at Widom line crossover. Nat. Commun. **10**, 4114 (2019)

[18] Pipich, V., Schwahn, D.: Densification of Supercritical Carbon Dioxide Accompanied by Droplet Formation When Passing the Widom Line. Phys. Rev. Lett. **120**, 145701 (2018)

[19] Nishikawa, K., Tanaka, I.: Correlation lengths and density fluctuations in supercritical states of carbon dioxide. J. Chem. Phys. Lett. **244**, 149–152 (1995)

[20] Arai, A.A., Morita, T., Nishikawa, K.: Investigation of structural fluctuation of supercritical benzene by Small-Angle X-ray Scattering. J. Chem. Phys. **119**, 1502–1509 (2003)

[21] Ploetz, E.A., Smith, P.E.: Gas or liquid? The supercritical behavior of pure fluids. J. Phys. Chem. B **123**, 6554 (2019)

[22] Brazhkin, V.V., Fomin, Y.D., Lyapin, A.G., Ryzhov, V.N., Trachenko, K.: Two Liquid States of Matter: A Dynamic Line on a Phase Diagram. Phys. Rev. E **85**, 031203 (2012)

[23] Bolmatov, D., Brazhkin, V.V., Trachenko, K.: Thermodynamic behaviour of supercritical matter. Nature Comm. **4**, 2331 (2013)

[24] Yang, C., Brazhkin, V.V., Dove, M.T., Trachenko, K.: Frenkel line and solubility maximum in supercritical fluids. Phys. Rev. E **91**, 012112 (2015)

[25] Prescher, C., Fomin, Y.D., Prakapenka, V.B., Stefanski, J., Trachenko, K., Brazhkin, V.V.: Experimental Evidence of the Frenkel Line in Supercritical Neon. Phys. Rev. B **95**, 134114 (2017)

[26] Proctor, J.E., Pruteanu, C.G., Morrison, I., Crowe, I.F., Loveday, J.S.: Transition from gas-like to liquid-like behavior in supercritical N_2. J. Phys. Chem. Lett. **10**, 6584–6589 (2019)

[27] Balucani, U., Zoppi, M.: Dynamics of the Liquid State. Clarendon Press, Oxford, U.K. (1995)

[28] Pearl, J.C., Conrath, B.J., Hanel, R.A., Pirraglia, J.A., Coustenis, A.: The albedo, effective temperature, and energy balance of Uranus, as determined from Voyager IRIS data. Icarus **84**, 12–28 (1990)

[29] Guillot, T.: Condensation of Methane, Ammonia, and Water and the Inhibition of Convection in Giant Planets. Science **269**, 1697–1699 (1995)

[30] de Pater, I., Sromovsky, L.A., Fry, P.M., Hammel, H.B., Baranec, C., Sayanagi, K.M.: Record-breaking storm activity on Uranus in 2014. Icarus **252**, 121–128 (2015)

[31] Setzmann, U., Wagner, W.: A new equation of state and tables of thermodynamic properties for methane covering the range from the melting line to 625 K at pressures up to 1000 MPa. J. Phys. Chem. Ref. Data **20**, 1061–1151 (1991)

[32] Chapman, S., Cowling, T.: The Mathematical Theory Of Non Uniform Gases. Cambridge University Press, Cambridge, U.K. (1952)

[33] Hansen, J.P., McDonald, I.: Theory of Simple Liquids, 3rd Edition. Academic Press, London, U.K. (2006)

[34] Kamgar-Parsi, B., Cohen, E.G.D., de Schepper, I.M.: Dynamical processes in hard-sphere fluids. Phys. Rev. A **35**, 4781 (1987)

[35] Heyes, D.M., Cass, M.J., Powles, J.G., Evans, W.A.B.: Self-Diffusion Coefficient of the Hard-Sphere Fluid: System Size Dependence and Empirical Correlations. J. Phys. Chem. B **111**, 1455–1464 (2007)

[36] Pieprzyk, S., Bannerman, M.N., Brańka, A.C., Chudak, M., Heyes, D.M.: Thermodynamic and dynamical properties of the hard sphere system revisited by molecular dynamics simulation. Phys. Chem. Chem. Phys. **21**, 6886–6899 (2019)

[37] Harris, K.R.: The density dependence of the self-diffusion coefficient of methane at –50°, 25° and 50°C. Physica **94A**, 448–464 (1978)

[38] Harris, K.R., Trappeniers, N.J.: The density dependence of the self-diffusion coefficient of liquid methane. Physica **104A**, 262–280 (1980)

[39] Carnahan, N.F., Starling, K.E.: Equation of State for Nonattracting Rigid Spheres. J. Chem. Phys. **51**, 635 (1969)

[40] Einstein, A.: Zur Theorie der Brownschen Bewegung. Ann. Phys. **324**, 371–381 (1906)

[41] Langevin, P.: Sur la théorie du mouvement brownien. C.R. Acad. Sci. Paris **146**, 530–533 (1908)

[42] Olsson, L.G., Larsson, K.E.: A comparative study of the motions of methane molecules and argon atoms in liquid and high-pressure gas states by neutron scattering. Physica **72**, 300–318 (1972)

[43] Ranieri, U., Klotz, S., Gaal, R., Koza, M.M., Bove, L.E.: Diffusion in dense supercritical methane from quasi-elastic neutron scattering measurements. Nature Comm. **12**, 1958 (2021)

[44] Ranieri, U., Koza, M.M., Kuhs, W.F., Klotz, S., Falenty, A., Gillet, P., Bove, L.E.: Fast methane diffusion at the interface of two clathrate structures. Nature Comm. **8**, 1076 (2017)

[45] Teixeira, J., Bellissent-Funel, M.C., Chen, S.H., Dianoux, A.J.: Experimental determination of the nature of diffusive motions of water molecules at low temperatures. Phys. Rev. A **31**, 1913–1917 (1985)

[46] Amann-Winkel, K., Bellissent-Funel, M.-C., Bove, L.E., Loerting, T., Nilsson, A., Paciaroni, A., Schlesinger, D., Skinner, L.: X-ray and neutron scattering of water. Chem. Rev. **116**, 7570–7589 (2016)

[47] Singwi, K.S., Sjölander, A.: Diffusive motions in water and cold neutron scattering. Phys. Rev. **119**, 863 (1960)

[48] Oosting, P.H., Trappeniers, N.J.: Proton-spin–lattice relaxation and self-diffusion in methanes: IV. Self-diffusion in methane. Physica **51**, 418–431 (1971)

[49] De Francesco, A., Guarini, E., Bafile, U., Formisano, F., Scaccia, L.: Bayesian approach to the analysis of neutron Brillouin scattering data on liquid metals. Phys. Rev. E **94**, 023305 (2016)

[50] Younglove, B.A., Ely, J.F.: Thermophysical properties of fluids. II. Methane, ethane, propane, isobutane, and normal butane. J. Phys. Chem. Ref. Data **16**, 577 (1987)

[51] Bell, I.H., Dyre, J.C., Ingebrigtsen, T.S.: Excess-entropy scaling in supercooled binary mixtures. Nature Comm. **11**, 4300 (2020)

[52] Lovesey, S.W.: The Theory of Neutron Scattering from Condensed Matter. Oxford University Press, Oxford, U.K. (1986)

[53] Bell, I.H., Delage-Santacreu, S., Hoang, H., Galliero, G.: Dynamic Crossover in Fluids: From Hard Spheres to Molecules. J. Phys. Chem. Lett. **12**, 6411 (2021)

[54] Xu, L., Kumar, P., Buldyrev, S.V., Chen, S.-H., Poole, P.H., Sciortino, F., Stanley, H.E.: Relation between the Widom line and the dynamic crossover in systems with a liquid–liquid phase transition. Proc. Natl Acad. Sci. USA **102**, 16558–16562 (2005)

[55] Bove, L.E., Dorner, B., Petrillo, C., Sacchetti, F., Suck, J.-B.: Neutron scattering investigation of low-momentum collective ion dynamics in liquid potassium. Phys. Rev. B **68**, 024208 (2003)

Methods

Experimental setup. The measurements have been carried out at the Institut Laue-Langevin large-scale facility in Grenoble, France, on the time-of-flight neutron spectrometer IN6-SHARP. We set the wavelength of the incoming neutron beam to 5.12 Å. Neutron scattering spectra of methane at 200±1 K were recorded at pressures between 8.5 and 2450 bar with a typical acquisition time of 3-4 hours per pressure point. The sample was contained in a cylindrical pressure cell of aluminium alloy whose height was about 50 mm and whose internal diameter was 6 mm, and was compressed using a gas compressor working with methane. In this setup, the sample volume does not change upon pressure increase/decrease and the number of methane molecules in the neutron beam increases with increasing pressure. To reduce the multiple scattering contributions, we inserted a cylindrical aluminium spacer of 5 mm in diameter for the measurements at the following eight pressures: 46, 97, 197, 349, 400, 650, 1275, and 2450 bar. The nine pressure points measured without aluminium spacer were: 8.5, 19, 25, 30, 40, 41.5, 51.5, 67.5, and 75.5 bar. The CH_4 (purity>99.95%) bottle was purchased from AirLiquide, Saint Priest, France. Pressure was directly measured by a manometer attached to the capillary connecting the gas compressor with the high-pressure cell. The uncertainty on the pressure measurement was 1 bar. The sample temperature was controlled using a standard "orange" cryostat. Empty-cell spectra were measured with and without aluminium spacer.

Data extraction and fitting. For each pressure point, constant-Q spectra from 0.4 to 1.5 $Å^{-1}$ with 0.1 $Å^{-1}$ steps were extracted (except in Fig. 1 where a larger integration range of 0.3 $Å^{-1}$ was used). Their intensity was normalized using the measurement of a vanadium standard and the empty-cell signal was subtracted using P- and Q-dependent transmission values (the spectra reported in Figs. 1 and 2 are empty cell-subtracted).

The different possible motions of methane (vibrations, rotations and translations) lie on different time scales. The contribution of the vibrational motion is very fast and can be approximated with a Debye–Waller factor. Rotations are too fast to be properly resolved on IN6-SHARP and probably only contribute as a very broad quasi-elastic signal appearing as a flat background in our spectra. Therefore, only the vibrational and translational motions were included in the fitting model, similarly to our previous QENS study of dense supercritical methane at 300 K [43]. The accessible energy range is inherently limited in time-of-flight neutron spectrometers and is rather narrow at small Q. For example, it goes from -2.2 to 1.8 meV at 0.5 $Å^{-1}$, as can be seen in Fig. 2. To limit the effect that the rotational contribution might have on our results, fits of the spectra at high Q were restricted over a reduced energy range.

Spectra are given in arbitrary units and were accordingly fitted using a Gaussian or Lorentzian function multiplied by a scaling factor in arbitrary units. A flat positive background B and a zero shift (small difference between the values of the true and nominal zeros of the energy transfer axis) were

included. Moreover, in the fitting of the spectra, convolution of $S_{\mathrm{self}}(Q,\omega)$ with the instrumental resolution function was taken into account. The resolution function of the spectrometer $R(E)$ was obtained by fitting the measurement of the vanadium standard to a pseudo-Voigt distribution. Its full width at half maximum was about 0.077 meV. Therefore, each constant-Q spectrum was fitted using either of the two formulas:

$$I^{\mathrm{Gauss}}(E) = I_0^{\mathrm{Gauss}} \exp\left(-\frac{\ln(2)(E-E_0)^2}{\hbar^2\Gamma_G^2}\right) \otimes R(E) + B_0, \tag{7}$$

$$I^{\mathrm{Lor}}(E) = \frac{I_0^{\mathrm{Lor}}}{\pi} \frac{\hbar\Gamma_L}{(E-E_0)^2 + \hbar^2\Gamma_L^2} \otimes R(E) + B_0. \tag{8}$$

Both Gaussian and Lorentzian fits have four parameters: I_0^{Gauss} or I_0^{Lor}, Γ_G or Γ_L, E_0, and B_0. The zero shift of the energy-transfer axis E_0 was generally left free to vary. However, it was systematically imposed at high Q in the Gaussian fits to an extrapolation of the small Q values (it would otherwise converge to relatively large values up to 0.2-0.3 meV). Similarly, to ensure a smooth Q dependence, the flat background B_0 was imposed to an extrapolation of the higher Q values at small Q values in the Gaussian fits and at the smallest Q only in the Lorentzian fits (it would otherwise converge to larger values). Supplementary Figs. 10 and 11 report all B_0 values. We checked that both of these choices (for zero shift and flat background) have only minor effects on the determination of the diffusion coefficient. Intensities and widths were always left as free parameters in the fitting. Supplementary Fig. 12 reports the fitted Lorentzian half widths at pressures where Gaussian fits were preferred and the fitted Gaussian half widths at pressures where Lorentzian fits were preferred (therefore complementing Fig. 3 of the main text).

The obtained intensities I_0^{Gauss} and I_0^{Lor} are plotted as a function of Q in Supplementary Fig. 13. They were fitted using:

$$I_0^{\mathrm{Gauss}} \propto \frac{1}{Q}\exp(-Q^2\langle u^2\rangle/3), \tag{9}$$

$$I_0^{\mathrm{Lor}} \propto \exp(-Q^2\langle u^2\rangle/3). \tag{10}$$

I_0^{Gauss} corresponds to the height of the Gaussian function before convolution with the instrumental resolution and is proportional to the factor $1/Q$ (see Eq. 3) multiplied by the Debye-Waller factor $\exp(-Q^2\langle u^2\rangle/3)$. I_0^{Lor} corresponds to the area of the Lorentzian function before convolution with the instrumental resolution and is simply proportional to the Debye-Waller factor. The resulting values of $\langle u^2\rangle^{1/2}$ are reported as a function of pressure in Supplementary Fig. 14. They amount to roughly 1 Å, which is a reasonable value and within the range of values reported in the literature for example of liquid water at ambient conditions, for which many QENS studies exist. We observe an increasing trend for $\langle u^2\rangle^{1/2}$ with increasing pressure (see Supplementary Fig. 14) in both estimations (from the Gaussian and Lorentzian intensities)

with a discontinuity between the Gaussian and Lorentzian estimations whose origin is presently unclear.

The Gaussian half widths were fitted over the Q range from 0.4 to 1.5 Å^{-1}, as shown in Fig. 3a. In the linear fits, the data points were not weighted according to the estimated error in $\Gamma_G(Q)$. This choice moderates the weight of the low-Q points (having the smaller error), corresponding to the regime where the theoretical ground for the Gaussian modelling is weaker. The Lorentzian half widths were fitted over a slightly narrower Q range from 0.4 to 1.3 Å^{-1} (Fig. 3b), similarly to our previous work [43], in order to limit the potential effect of the rotational contribution. This is because the rotational contribution i) becomes slower with increasing pressure and might potentially approach the timescale window accessible by the present experiment at our highest pressures and ii) is known from analytical modelling to have increasing intensity with increasing Q. The data points were weighted according to the estimated error in $\Gamma_L(Q)$.

Finally, multiple scattering contributions to the spectra were ignored. The multiple scattering was calculated following the established procedure described in ref. [55] for a few selected pressure points and its subtraction was observed to have negligible effect on the fits and on the determination of the diffusion coefficient. This test was performed at three pressures: 67.5 bar (measured without the aluminium spacer in the high-pressure cell containing the sample), and 97 and 1275 bar (both measured with the spacer). The calculated multiple scattering is much weaker and broader than the single scattering and included in the flat background over the considered energy range. This is confirmed by the observation that there is no inconsistency between the results for the data measured with and without the aluminium spacer. In particular, the results for the point at 46 bar, which was measured with the spacer, perfectly interpolate in between the results for 41.5 and 51.5 bar, which were measured without the spacer.

Data availability

Data were generated at the Institut Laue-Langevin large-scale facility and are stored on the ILL data portal under doi 10.5291/ILL-DATA.6-01-332.

Acknowledgments

We acknowledge the Institut Laue-Langevin for provision of beam time and Claude Payre, James Maurice, Eddy Lelièvre-Berna, Jean Marc Zanotti, and Quentin Berrod for advice and technical assistance during the experiment. We acknowledge Ubaldo Bafile and José Teixeira for useful discussions on the data analysis, and L. Scaccia for her contribution to the Bayesian code.

Author contributions

The project was conceived by F.F, F.A.G, M.S. and L.E.B.. The experiments were performed by F.F., F.A.G., M.S., M.M.K., and L.E.B.. New analytic tools

have been provided by F.F. and L.E.B. The data were analysed and the figures produced by U.R., with contributions from F.F. and L.E.B.. F. F performed the Bayesian analysis using the code written by A.D.F.. The manuscript was written by U.R. and L.E.B.. All authors discussed the results and commented on the manuscript.

Competing interests

The authors declare no competing interests.

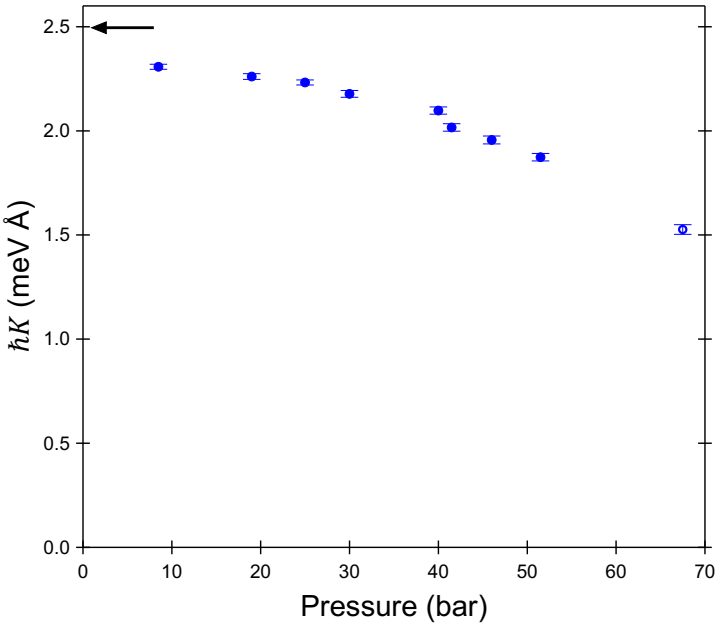

Extended Data Fig. 1 | Slope parameter K appearing in Eq. 4. Pressure dependence of the slope of the linear fits of the Gaussian half widths shown in Fig. 3a. 67.5 bar is also included. The arrow indicates the value calculated from the theoretical expression for ballistic diffusion (Eq. 1): $K{=}(2\ln(2)k_{\mathrm{B}}T/m)^{1/2}$.

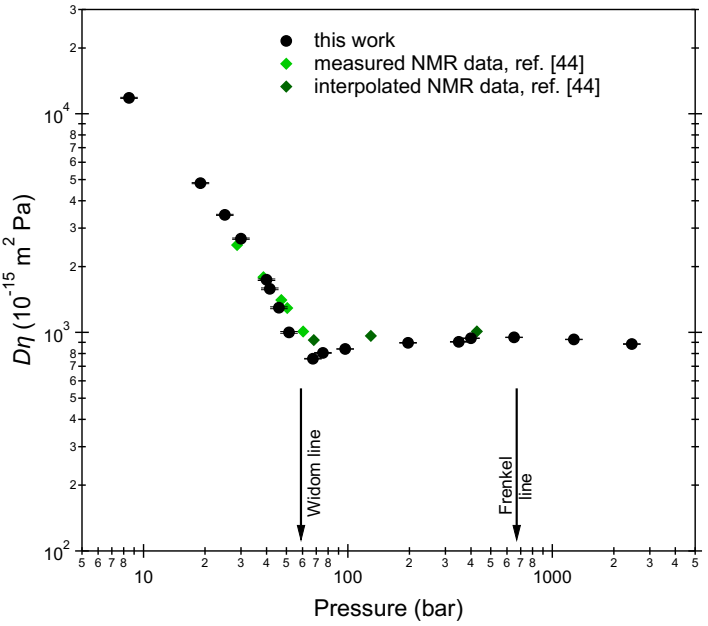

Extended Data Fig. 2 | Test of the Stokes–Einstein–Sutherland relation. Pressure dependence of the product between the self-diffusion coefficient D at 200 K (from this work and from ref. [48]) and the viscosity η at the same temperature from the equation of state-like viscosity model of ref. [50]. The error bars were obtained by propagating the errors in D only. The Stokes–Einstein–Sutherland relation predicts a constant product $D\eta$ along isotherms.